Gas-Phase Reactions

International Edition: DOI: 10.1002/anie.201606259
German Edition: DOI: 10.1002/ange.201606259

Efficient Room-Temperature Activation of Methane by TaN^+ under C–N Coupling

*Shaodong Zhou, Jilai Li, Maria Schlangen, and Helmut Schwarz**

Dedicated to Gerhard Ertl on the occasion of his 80th birthday

Abstract: *The thermal reaction of diatomic tantalum nitride cation $[TaN]^+$ with methane has been explored using FT-ICR mass spectrometry complemented by high-level quantum chemical calculation; based on this combined experimental/computational approach, mechanistic aspects of this novel, highly efficient C–N coupling process have been uncovered. In distinct contrast to $[TaN]^+$, its lighter congeners $[VN]^+$ and $[NbN]^+$ are inert towards methane under ambient conditions, and the origins of the remarkably variable efficiencies of the three metal nitrides are uncovered by CCSD(T) calculations.*

Gas-phase activation of methane under C–N coupling is important to convert this abundantly available feedstock into value-added commodities;[1] for example, this task has been accomplished in the large-scale DEGUSSA (BMA)[2] and the Andrussow[3] processes for producing hydrogen cyanide [Equations (1) and (2), respectively].

$$CH_4 + NH_3 \rightarrow HCN + 3\,H_2 \quad (1)$$

$$CH_4 + NH_3 + 1.5\,O_2 \rightarrow HCN + 3\,H_2O \quad (2)$$

Despite the enormous economic importance of these transformations, there are only a few studies aimed at elucidating the mechanistic aspects of methane activation, accompanied with C–N coupling, at a strictly molecular level in the gas phase.[1b] For example, to mimic the DEGUSSA process, bare atomic and platinum cluster ions have been allowed to react with methane and ammonia. Generation of a platinum carbene intermediate was identified as the key step, and C–N coupling is brought about by nucleophilic addition of NH_3 to the methylene ligand.[4] This sequence of events, however, is not confined to M = Pt; also the atomic transition-metal cations Rh^+, W^+, Os^+, Ir^+, and Au^+ are capable to mediate this transformation.[5] Further, C–N coupling of methane and ammonia promoted by Pt-based hetero-bimetallic clusters has also been explored, and the diatomic platinum-coinage metal ions $[PtM]^+$ (M = Cu, Ag, Au)[6] proved particularly active. While the carbene complexes of homonuclear larger platinum clusters also react with ammonia, C–N coupling does not take place; rather, NH_3 will coordinate to the polynuclear metal core accompanied by dehydrogenation of the methylene ligand.[7]

In addition to the above mentioned processes, C–N coupling in the gas phase was also observed for a few other systems.[1b,8] For example, while $[NiCH]^+$ reacts with ammonia to generate the products $Ni/[CH_2NH_2]^+$, $[Ni,C,H_2,N]^+/H_2$, and $[Ni,C,H_3,N]^+/H$,[9] the carbyne complexes $[Pt_nCH]^+$ ($n = 1, 2$) give rise to the formation of $Pt_n/[CH_2NH_2]^+$, $[Pt_n,C,H_2,N]^+/H_2$, and Pt_nC/NH_4^+ under the same conditions.[10] Further, the $[MCH_3]^+$ ions (M = Zn, Cd, Hg) react with ammonia in a rather unusual gas-phase S_N2 process to give $M/[CH_3NH_3]^+$ and, additionally, the long-lived encounter complex $[M(CH_3)(NH_3)]^+$.[11] C–N coupling has also been noted in the thermal reaction of $[Ni(NH_2)]^+$ with C_2H_4 to form $Ni/[C_2H_6N]^+$ and $[Ni(C_2H_4N)]^+/H_2$.[12] Finally, an unprecedented alkyne/nitrile gas-phase metathesis was observed for the high-valent iron nitrido dication $[LFeN]^{2+}$ when treated with alkynes to form RCN and $[LFe(CR)]^+$.[13]

Herein, we report that at ambient conditions cationic tantalum nitride $[TaN]^+$ activates methane rather efficiently under C–N coupling to generate exclusively $[Ta(NCH_2)]^+/H_2$. This behavior is in distinct contrast to that of its lighter congeners, $[VN]^+$ and $[NbN]^+$, which are inert towards methane under the same conditions. Mechanistic aspects of the reactions are described, and the origins of the rather varying reactivities of the $[MN]^+/CH_4$ (M = V, Nb, Ta) couples are discussed.

Mass-selected and thermalized $[TaN]^+$ reacts with CH_4 to afford $[Ta,C,H_2,N]^+/H_2$ as the sole product ion, Figure 1 a and Equation (3) (for technical details, see the Supporting Information); the reaction efficiency amounts to $\phi = 50\,\%$, relative to the collision rate,[14] with a rate constant of $k = (3.1 \pm 0.9) \times 10^{-10}\,cm^3\,molecule^{-1}\,s^{-1}$. Owing to the uncertainty in the determination of the absolute pressure, an error of $\pm 30\,\%$ is associated with these measurements.[15] In the reaction of $[TaN]^+$ with CD_4, the rate constant did not change within detection limit; thus, isotopic substitution has no effect on the reaction rate. However, when $[TaN]^+$ is treated with CH_2D_2, the neutral products H_2, HD, and D_2 are formed in a ratio of 1:3.3:0.7. Thus, an intramolecular kinetic isotope effect of KIE = 1.2 affects the branching ratio. Finally, when mass-selected $[Ta,C,H_2,N]^+$ is subjected to collisional activation (CA), up to a collision energy of $E_{coll} = 7.8$ eV, only Ta^+ is

$$[TaN]^+ + CH_4 \rightarrow [Ta,C,H_2,N]^+ + H_2 \quad (3)$$

[*] Dr. S. Zhou, Prof. Dr. J. Li, Dr. M. Schlangen, Prof. Dr. H. Schwarz
Institut für Chemie, Technische Universität Berlin
Strasse des 17. Juni 135, 10623 Berlin (Germany)
E-mail: helmut.schwarz@tu-berlin.de
Prof. Dr. J. Li
Institute of Theoretical Chemistry, Jilin University
Changchun, 130023 (P.R. China)

Supporting information for this article can be found under: http://dx.doi.org/10.1002/anie.201606259.

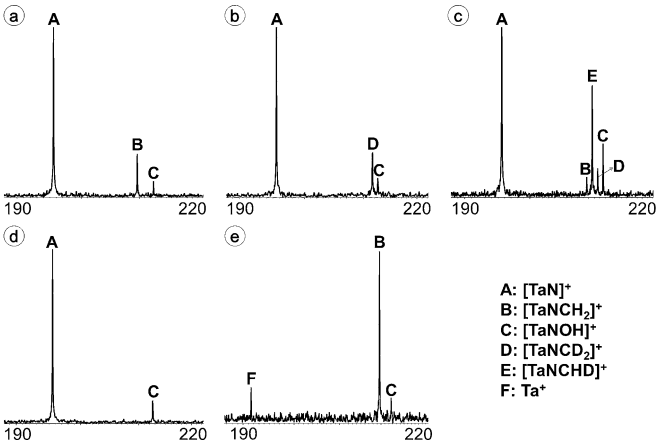

Figure 1. Mass spectra of the thermal reactions of mass-selected $[TaN]^+$ with methane: a) CH_4, b) CD_4, d) Ar; all with a reaction delay of 2 s, and c) CH_2D_2 with a reaction delay of 5 s ($p = 2\times10^{-9}$ mbar); e) CA spectrum for $[Ta,C,H_2,N]^+$ upon collision with Ar at $E_{coll} = 7.8$ eV; the signal labeled as **C** is due to the reaction of $[TaN]^+$ with background water; the longer reaction delay for the couple $[TaN]^+/CH_2D_2$, spectrum (c), was used to detect all isotopic variants.

generated; this finding points to the presence of an intact "CH_2N" ligand.

Next, the reaction mechanisms were interrogated by quantum chemical calculations. The potential-energy surfaces (PESs) of the most favorable reaction pathways as well as some structural information of relevant species are shown in Figure 2 and Figure 3. Figure 2 refers to the initial phase of the ion/molecule reaction, while Figure 3 deals with the liberation of molecular hydrogen.

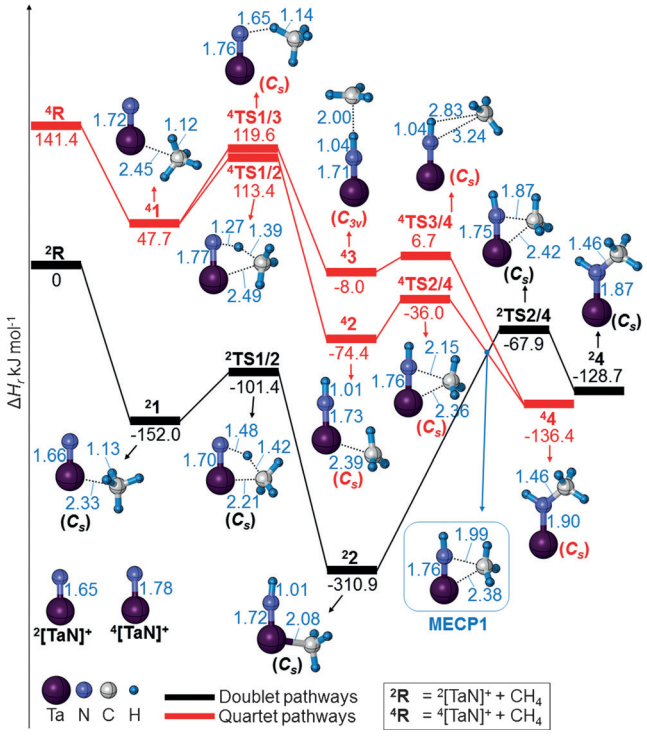

Figure 2. PES and selected structural information for the generation of $[Ta(NHCH_3)]^+$ from $[TaN]^+/CH_4$ as calculated at the CCSD(T)//BSII//PBE0/BSI level of theory. Zero-point corrected, relative energies are given in kJ mol^{-1} and bond lengths in Å; charges are omitted for the sake of clarity.

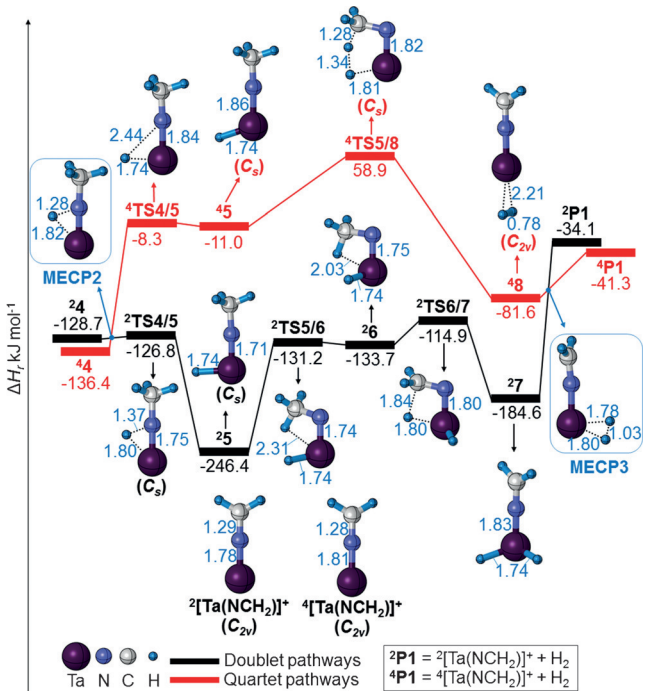

Figure 3. The energetically most favorable PES and selected structural information for the generation of $[Ta(NCH_2)]^+$ from **4** as calculated at the CCSD(T)/BSII//PBE0/BSI level of theory. Zero-point corrected, relative energies are given in kJ mol^{-1} and bond lengths in Å; charges are omitted for the sake of clarity.

Two spin states of $[TaN]^+$ had to be considered. While doublet $^2[TaN]^+$ corresponds to the ground state, it will be shown that also the excited quartet state plays a role in the generation of the $[Ta(NHCH_3)]^+$ intermediate (Figure 2), and its dehydrogenation (Figure 3). As shown in Figure 2, formation of $[Ta(NHCH_3)]^+$ can occur on the doublet PES. Thus, starting from the encounter complex ^{2}**1**, the insertion of $^2[TaN]^+$ into the H_3C–H bond takes place via ^{2}**TS1/2** to form the rather stable intermediate ^{2}**2**. Next, the newly formed methyl group rebinds to the N atom via ^{2}**TS2/4** to generate $^2[Ta(NHCH_3)]^+$ (^{2}**4**); both transition states are lower in energy compared to the ground-state entrance channel (^{2}**R**). Liberation of the methyl ligand from ^{2}**2** to produce $[TaNH]^+ + CH_3^{\cdot}$ is calculated to be 17 kJ mol^{-1} higher in energy relative to ^{2}**R**, and is thus inaccessible under thermal conditions.

The "insertion-rebound" pathway has also been located on the quartet surface, that is, ^{4}**R** → ^{4}**1** → ^{4}**TS1/2** → ^{4}**2** → ^{4}**TS2/4** → ^{4}**4**. Thus, starting from ^{4}**1**, a conventional hydrogen-atom transfer (HAT)[16] from CH_4 to the N-atom takes place via ^{4}**TS1/3** to generate ^{4}**3**, which is to be followed by a rebound of the methyl group to form $^4[Ta(NHCH_3)]^+$ (^{4}**4**). This HAT pathway profits from the high spin density at the N-atom of $^4[TaN]^+$ (0.6). However, all intermediates and transition

structures of the quartet PES are higher in energy as compared to the doublet species except for the C–N coupling intermediate **4**, which possesses a quartet ground state (^{4}**4**). Thus, a minimum energy crossing point (MECP)[17] has been searched for and was located between **2** and **4** (9 kJ mol^{-1} below ^{2}**TS2/4**); at **MECP1** the doublet and quartet surfaces intersect.

As shown in Figure 3, dehydrogenation of the CH_3NH ligand attached to Ta^+ preferably proceeds via consecutive activations of the N–H and C–H bonds, again involving both the doublet and quartet spin states. On the doublet PES, a hydrogen-atom is first transferred from N to Ta via ^{2}**TS4/5** to form ^{2}**5**; the second transfer of a hydrogen atom from the methyl group is achieved via two steps, that is, ^{2}**5**→^{2}**6**→^{2}**7**. Although ^{2}**7** corresponds to a genuine metal dihydride ($d_{H\text{-}H}$ = 2.77 Å), molecular hydrogen can be eliminated from this complex directly without imposing a barrier according to a relaxed scan of the H-Ta-H angle to produce ^{2}[Ta-(CH_2N)]$^+$ + H_2 (^{2}**P1**). The N–H/C–H bond transformations on the quartet surface are similar to the ones on the doublet surface except that only two steps, ^{4}**4**→^{4}**5**→^{4}**8**, are involved; the intermediate **6** which on the doublet surface is stabilized by agostic interaction has not been located on the quartet PES. In addition, ^{4}**8** corresponds to a dihydrogen complex ($d_{H\text{-}H}$ = 0.81 Å). Comparing the overall processes **4**→→**P1** for the two spin-state surfaces, the quartet species are in general much higher in energy than those on the doublet potential surface except for ^{4}**4** and ^{4}**P1**. Thus, at least two additional MECPs exist on the PESs: **MECP2** is located between **4** and **TS4/5** (1 kJ mol^{-1} below ^{2}**TS4/5**), and **MECP3** matters in the final step ^{2}**7**→^{2}**P1** (105 kJ mol^{-1} above ^{2}**7**).

For the overall reaction from **R** to **P1** the energetically most favorable route involves a two-state reactivity (TSR)[18] scenario, that is, ^{2}**R**→^{2}**1**→^{2}**2**→**MECP1**→^{4}**4**→**MECP2**→^{2}**5**→^{2}**6**→^{2}**7**→**MECP3**→^{4}**P1**. However, the spin-crossings are not essential to produce [Ta(NCH_2)]$^+$, as the doublet pathway itself is available under thermal conditions. In any case, for both the TSR and a single-spin state reactivity (SSR) scenario, the elimination of molecular hydrogen from ^{2}**7** corresponds to the rate-limiting step; this is in line with the intermolecular KIE = 1, as determined experimentally from the [TaN]$^+$/CH_4/CD_4 couples. The KIE = 1.2 which affects the branching ratio for the production of H_2/HD/D_2 from [TaN]$^+$/CH_2D_2 is, most likely, due to the barriers involved in the various intra-complex H/D migrations via **1**→**2**→**3**→**4**→**5**→**6**→**7**.

In addition to the pathways presented in Figure 2 and Figure 3, several other possible reaction scenarios have been considered theoretically, for example, dehydrogenation of the CH_3NH ligand via a sequence of first C–H and then N–H bond cleavage, as well as pathways for producing the isomeric complex [Ta(NHCH)]$^+$. However, these routes are much less competitive energetically (for more details, see the Supporting Information). With regard to other conceivable products, for example, [(H_2C)TaN]$^+$ and [(HC)Ta(NH)]$^+$, both are calculated to be higher in energy than ^{2}**R** (63 kJ mol^{-1} and 5 kJ mol^{-1}, respectively); thus, they are inaccessible at ambient conditions.

To explore the scope and limitations of this selective C–N coupling process, we have also generated the two nitrides [VN]$^+$ and [NbN]$^+$; both species are, however, unreactive towards methane under the same conditions as employed for [TaN]$^+$/CH_4. Computational results suggest that the pathways for the initial H_3C–H bond activation by [MN]$^+$ (M = V, Nb) resemble mechanistically those for [TaN]$^+$/CH_4; the respective energetic data are shown in Table 1 (for structural information, see Supporting Information). However, the inspection of the data clearly indicates that even the most favorable initial step, ^{2}**R**→^{2}**1**→^{2}**TS1/2**→^{2}**2**, is inaccessible for [MN]$^+$/CH_4 (M = V, Nb) as ^{2}**TS1/2** is for both couples located above ^{2}**R**. This result is in line with the experimental findings.

Table 1: Energetics for bond activation reactions of the systems [MN]$^+$/CH_4 (M = V, Nb).[a]

Species	ΔH_r, kJ mol^{-1}	
	M = V	M = Nb
^{2}**R**	0	0
^{2}**1**	−98.0	−92.1
^{2}**TS1/2**	8.4	25.7
^{2}**2**	−83.7	−145.9
^{4}**R**	196.2	215.9
^{4}**1**	107.5	125.6
^{4}**TS1/2**	–[b]	193.7
^{4}**2**	–[b]	25.5
^{4}**TS1/3**	170.6	254.6
^{4}**3**	117.4	122.9

[a] For structural representations, see the Supporting Information.
[b] These species were not located for [VN]$^+$/CH_4.

When comparing the pathways ^{2}**R**→^{2}**1**→^{2}**TS1/2**→^{2}**2** for the three couples, for [TaN]$^+$/CH_4 all three species ^{2}**1**, ^{2}**TS1/2**, and ^{2}**2** are much lower in energy than those calculated for [VN]$^+$/CH_4 and [NbN]$^+$/CH_4, respectively. This is due to a much stronger Ta–C interaction as compared to the V–C and Nb–C interactions. Most likely, lanthanide contraction leads to tightening of the valence s and p orbitals thus resulting in stronger metal–carbon bonds for 5d metals.[19] As analyzed earlier in a broader context, these features originate from the operation of strong relativistic effects.[20] The stronger Ta–C interaction is reflected by the BDE-((HN)Ta^+–CH_3) (ca. 328 kJ mol^{-1}), which is considerably higher than BDE((HN)V^+–CH_3) (ca. 236 kJ mol^{-1}), and BDE((HN)Nb^+–CH_3) (ca. 294 kJ mol^{-1}), respectively. Accordingly, for the tantalum-containing systems, ^{2}**1**, ^{2}**TS1/2**, and ^{2}**2** are more energetically favorable on the PES. Moreover, an NBO analysis provides further insight. In all ^{2}[MN]$^+$ cations investigated (M = V, Nb, Ta), the N atom is bound to the metal core via one σ- and two π-bonds, and one unpaired electron is located in the 5d orbital of the metal. The occupancies and characters of these orbitals do not change during the step ^{2}**1**→^{2}**2**, that is, they serve as innocent spectators. In contrast, the 2s electron lone pair of the nitrogen atom in ^{2}**1** is transformed to a σ(N–H) orbital in ^{2}**2** when making the N–H bond; the electron pair of the original H_3C–H bond has been transferred to a σ(M–C) orbital to form the M–C bond. Thus, the process ^{2}**1**→^{2}**2** has all the features of a proton-coupled electron transfer (PCET).[21] Accordingly, the higher electron density at the N atom of

$^2[TaN]^+$ (charge on N: −0.56) as compared to that of $^2[VN]^+$ (charge on N: −0.29) and of $^2[NbN]^+$ (charge on N: −0.45) favors accepting a proton from methane; this effect also contributes to the high reactivity of the $[TaN]^+/CH_4$ couple as compared to its lighter congeners.

In summary, we have presented a novel example for a highly efficient thermal activation of methane by $[TaN]^+$ and uncovered details of the mechanistic scenarios for an "insertion-coupling" process that eventually generates $[Ta(NCH_2)]^+$. While the TSR pathway involves three MECPs to form the energetically most favorable products, a SSR channel is also available under thermal conditions. In distinct contrast to the high reactivity of $[TaN]^+$, its lighter congeners $[VN]^+$ and $[NbN]^+$ are inert towards methane; this inertness can be traced back to relativistic effects and a higher ionic character of $[TaN]^+$. The relativistic effects results in a much stronger Ta–C interaction, and the higher ionic character facilitates the operation of PCET in the initial H_3C–H bond activation.

Acknowledgments

Generous financial support by the Fonds der Chemischen Industrie and the Deutsche Forschungsgemeinschaft ("UniCat") is appreciated. We thank Dr. Thomas Weiske for technical assistance.

Keywords: C–N coupling · gas-phase reactions · methane activation · quantum chemical calculations · tantalum nitride

How to cite: *Angew. Chem. Int. Ed.* **2016**, *55*, 11678–11681
Angew. Chem. **2016**, *128*, 11851–11855

[1] a) R. Horn, R. Schlögl, *Catal. Lett.* **2015**, *145*, 23–39; b) "Mechanisms of Metal-Mediated C-N Coupling Processes: A Synergistic Relationship between Gas-Phase Experiments and Computational Chemistry": R. Kretschmer, M. Schlangen, H. Schwarz in *Understanding Organometallic Reaction Mechanisms and Catalysis* (Ed.: V. P. Ananikov), Wiley-VCH, Weinheim, **2014**, pp. 1–16.

[2] a) A. Bockholt, I. S. Harding, R. M. Nix, *J. Chem. Soc. Faraday Trans.* **1997**, *93*, 3869–3878; b) D. Hasenberg, L. D. Schmidt, *J. Catal.* **1986**, *97*, 156–168.

[3] a) L. Andrussow, *Angew. Chem.* **1935**, *48*, 593–595; b) L. Andrussow, *Ber. Dtsch. Chem. Ges.* **1927**, *60*, 2005–2018.

[4] M. Aschi, M. Brönstrup, M. Diefenbach, J. N. Harvey, D. Schröder, H. Schwarz, *Angew. Chem. Int. Ed.* **1998**, *37*, 829–832; *Angew. Chem.* **1998**, *110*, 858–861.

[5] M. Diefenbach, M. Brönstrup, M. Aschi, D. Schröder, H. Schwarz, *J. Am. Chem. Soc.* **1999**, *121*, 10614–10625.

[6] a) K. Koszinowski, D. Schröder, H. Schwarz, *Angew. Chem. Int. Ed.* **2004**, *43*, 121–124; *Angew. Chem.* **2004**, *116*, 124–127; b) K. Koszinowski, D. Schröder, H. Schwarz, *J. Am. Chem. Soc.* **2003**, *125*, 3676–3677.

[7] a) K. Koszinowski, D. Schröder, H. Schwarz, *Organometallics* **2004**, *23*, 1132–1139; b) K. Koszinowski, D. Schröder, H. Schwarz, *Organometallics* **2003**, *22*, 3809–3819.

[8] R. Kretschmer, M. Schlangen, H. Schwarz, *Chem. Eur. J.* **2012**, *18*, 40–49.

[9] R. Kretschmer, M. Schlangen, H. Schwarz, *Dalton Trans.* **2013**, *42*, 4153–4162.

[10] B. Butschke, H. Schwarz, *Chem. Eur. J.* **2011**, *17*, 11761–11772.

[11] a) R. Kretschmer, M. Schlangen, M. Kaupp, H. Schwarz, *Organometallics* **2012**, *31*, 3816–3824; b) R. Kretschmer, M. Schlangen, H. Schwarz, *Angew. Chem. Int. Ed.* **2011**, *50*, 5387–5391; *Angew. Chem.* **2011**, *123*, 5499–5503.

[12] R. Kretschmer, M. Schlangen, H. Schwarz, *Angew. Chem. Int. Ed.* **2012**, *51*, 3483–3488; *Angew. Chem.* **2012**, *124*, 3541–3546.

[13] a) J. P. Boyd, M. Schlangen, A. Grohmann, H. Schwarz, *Helv. Chim. Acta* **2008**, *91*, 1430–1434; b) for other, intracomplex C–N coupling processes, of high-valent $[LFeN]^{2+}$, see: M. Schlangen, J. Neugebauer, M. Reiher, D. Schröder, J. P. López, M. Haryono, F. W. Heinemann, A. Grohmann, H. Schwarz, *J. Am. Chem. Soc.* **2008**, *130*, 4285–4294.

[14] M. T. Bowers, J. B. Laudenslager, *J. Chem. Phys.* **1972**, *56*, 4711–4712.

[15] D. Schröder, H. Schwarz, D. E. Clemmer, Y. M. Chen, P. B. Armentrout, V. I. Baranov, D. K. Bohme, *Int. J. Mass Spectrom. Ion Processes* **1997**, *161*, 175–191.

[16] For recent Reviews on HAT, see: a) M. Salamone, M. Bietti, *Acc. Chem. Res.* **2015**, *48*, 2895–2903; b) H. Schwarz, *Chem. Phys. Lett.* **2015**, *629*, 91–101; c) C. T. Saouma, J. M. Mayer, *Chem. Sci.* **2014**, *5*, 21–31; d) N. Dietl, M. Schlangen, H. Schwarz, *Angew. Chem. Int. Ed.* **2012**, *51*, 5544–5555; *Angew. Chem.* **2012**, *124*, 5638–5650; e) W. Z. Lai, C. S. Li, H. Chen, S. Shaik, *Angew. Chem. Int. Ed.* **2012**, *51*, 5556–5578; *Angew. Chem.* **2012**, *124*, 5652–5676; f) X. L. Ding, X. N. Wu, Y. X. Zhao, S. G. He, *Acc. Chem. Res.* **2012**, *45*, 382–390; g) J. M. Mayer, *Acc. Chem. Res.* **2011**, *44*, 36–46.

[17] J. N. Harvey, M. Aschi, H. Schwarz, W. Koch, *Theor. Chem. Acc.* **1998**, *99*, 95–99.

[18] a) J. N. Harvey, *WIREs Comput. Mol. Sci.* **2014**, *4*, 1–14; b) S. Shaik, *Int. J. Mass Spectrom.* **2013**, *354*, 5–14; c) S. Shaik, H. Hirao, D. Kumar, *Acc. Chem. Res.* **2007**, *40*, 532–542; d) W. Nam, *Acc. Chem. Res.* **2007**, *40*, 522–531; e) P. E. M. Siegbahn, T. Borowski, *Acc. Chem. Res.* **2006**, *39*, 729–738; f) S. Shaik, D. Kumar, S. P. de Visser, A. Altun, W. Thiel, *Chem. Rev.* **2005**, *105*, 2279–2328; g) H. Schwarz, *Int. J. Mass Spectrom.* **2004**, *237*, 75–105; h) S. Shaik, S. P. de Visser, F. Ogliaro, H. Schwarz, D. Schröder, *Curr. Opin. Chem. Biol.* **2002**, *6*, 556–567; i) D. Schröder, S. Shaik, H. Schwarz, *Acc. Chem. Res.* **2000**, *33*, 139–145; j) S. Shaik, M. Filatov, D. Schröder, H. Schwarz, *Chem. Eur. J.* **1998**, *4*, 193–199; k) P. B. Armentrout, *Science* **1991**, *251*, 175–179.

[19] a) S. Zhou, J. Li, M. Schlangen, H. Schwarz, *Chem. Eur. J.* **2016**, *22*, 7225–7228; b) J. J. Carroll, J. C. Weisshaar, *J. Phys. Chem.* **1996**, *100*, 12355–12363; c) K. K. Irikura, J. L. Beauchamp, *J. Phys. Chem.* **1991**, *95*, 8344–8351; d) J. A. M. Simoes, J. L. Beauchamp, *Chem. Rev.* **1990**, *90*, 629–688.

[20] a) P. Pyykkö, *Annu. Rev. Phys. Chem.* **2012**, *63*, 45–64; b) H. Schwarz, *Angew. Chem. Int. Ed.* **2003**, *42*, 4442–4454; *Angew. Chem.* **2003**, *115*, 4580–4593; c) K. K. Irikura, J. L. Beauchamp, *J. Am. Chem. Soc.* **1991**, *113*, 2769–2770.

[21] For recent Reviews on PCET, see a) S. Hammes-Schiffer, *J. Am. Chem. Soc.* **2015**, *137*, 8860–8871; b) A. Migliore, N. F. Polizzi, M. J. Therien, D. N. Beratan, *Chem. Rev.* **2014**, *114*, 3381–3465; c) D. R. Weinberg, C. J. Gagliardi, J. F. Hull, C. F. Murphy, C. A. Kent, B. C. Westlake, A. Paul, D. H. Ess, D. G. McCafferty, T. J. Meyer, *Chem. Rev.* **2012**, *112*, 4016–4093; d) J. J. Warren, T. A. Tronic, J. M. Mayer, *Chem. Rev.* **2010**, *110*, 6961–7001; e) P. E. M. Siegbahn, M. R. A. Blomberg, *Chem. Rev.* **2010**, *110*, 7040–7061; f) S. Hammes-Schiffer, *Chem. Rev.* **2010**, *110*, 6937–6938.

Received: June 28, 2016
Published online: August 11, 2016

